JOURNAL OF PROPULSION AND POWER
Vol. 15, No. 3, May–June 1999

Low-Power Helium Pulsed Arcjet

Gary F. Willmes* and Rodney L. Burton†
University of Illinois at Urbana–Champaign, Urbana, Illinois 61801

An electrothermal thruster that operates in a rapid-pulse mode at low power (<200 W) is investigated. The thruster, called a pulsed arcjet, uses a capacitor and a pulse-forming electrical circuit to transfer stored electrical energy to a propellant gas in 3–10 μs arc discharges at repetition rates of 550–2630 pulses-per-second. Peak currents in the arc are 110–270 A with pulse energies from 24 to 132 mJ. High-current diodes across the capacitor terminals are used to eliminate current reversals, and >85% of the initial stored energy is transferred to the arc in a unipolar pulse. The arc discharges occur in a cylindrical capillary upstream of a converging–diverging nozzle, and all of the energy addition occurs in the subsonic region. Tests with helium propellant are conducted for two 20-deg half-angle conical nozzles with area ratios of 20 and 230. Thrust levels from 14 to 31 mN are measured, and a maximum specific impulse of 313 s is achieved with 36% efficiency at 119 W. A time-dependent, quasi-one-dimensional numerical model is developed to evaluate energy losses using a time-marching procedure, and comparison with experimental results is good. Heat transfer losses to the wall in the subsonic region are found to be the primary energy-loss mechanisms. Specific impulse is strongly affected by wall temperature. Viscous effects become important as the specific energy increases above 12 MJ/kg and the throat Reynolds number falls below 1×10^3.

Nomenclature

A = area, m^2
C = capacitance, F
D = diameter, m
D_F = capacitor dissipation factor
d = breakdown length, m
E = energy, J; electric field strength, V/m
e = specific energy, J/kg
f = friction factor; frequency, Hz
g = standard gravity, m/s
h = enthalpy, J/kg
I = arc current, A
L = inductance, H; capillary length, m
m = propellant mass, kg
$\dot{m}$ = mass flow rate, kg/s
n = gas number density, m^{-3}
P = power, W
p = pressure, Pa
Q = heat transfer rate, W
q = heat transfer rate per unit mass, W/kg
R = resistance, Ω
r_0 = arc channel radius, m
T = temperature, K; thrust, N
U_{EQ} = equivalent exhaust velocity, m/s
u = flow velocity, m/s
V = voltage, V
γ = secondary emission coefficient
η = thrust efficiency, %
κ = thermal conductivity, W/m-K
ρ = density, kg/m^3
σ = electrical conductivity, Ω

Introduction

THE objective of this work is to develop a technique for extending the power range of an arcjet-type thruster to power levels below 200 W. The basic concept is to use a pulsed discharge rather than a dc arc to avoid some of the stability and scaling problems associated with low-power steady arcs. The origins of the pulsed arcjet come from work performed by Burton et al.,[1,2] on the pulsed electrothermal thruster (PET) in the 1980s. The development of the PET involved liquid water propellant with its associated two-phase flow problems, and one conclusion of the experimental work was that a switch to a gaseous propellant might be beneficial. While the PET operated at low frequency, 2–40 pulses-per-second (pps), with high pulse energies, 40–70 J, the pulsed arcjet investigated here operates at high frequency, 550–2630 pps, with low pulse energies, 24–132 mJ. Initial pulsed arcjet tests were conducted using simulated hydrazine propellant ($N_2 + 2H_2$); however, the performance did not appear promising, and the range of test conditions was restricted by the unfavorable breakdown characteristics of the diatomic gases. The performance and operating characteristics greatly improved with helium and allowed clear performance trends to be obtained experimentally. The experimental part of this research includes measurements of average thrust and power, as well as arc current and voltage for individual discharges. A numerical model is developed to identify the energy loss mechanisms and assess approaches for improving performance.

A helium pulsed arcjet thruster could potentially be used for stationkeeping or deorbiting satellites that have helium onboard for cryogenic cooling or when a nontoxic alternative to a hydrazine system is desired. While helium is an attractive propellant for its low molecular weight and high frozen-flow efficiency, on-orbit storage remains a difficult problem. Hence, little work has been done on helium-propellant arcjets, although the NASA 1-kW laboratory arcjet has been operated with helium at ~500–700 W input power.[3]

An arc discharge is produced using a constant-current power supply, a storage capacitor, and a pulse-forming electrical circuit (Fig. 1), directly coupled to the thruster electrodes. The power supply ramps up the voltage and stored energy on the capacitor until the propellant breakdown voltage is reached, initiating an arc discharge in a small-diameter, cylindrical capillary between the electrodes. The energy stored on the capacitor is transferred to the propellant gas in a short intense pulse. The arc attaches to the nozzle upstream of the convergent section, and the heat addition to the gas is entirely subsonic. The arc completely extinguishes when the voltage on the capacitor is not sufficient to maintain conduction, and the charging cycle repeats. A schematic of an ideal charge/discharge cycle is shown in Fig. 2. Utilizing the self-breakdown of the propellant eliminates the need for a switch or spark igniter, greatly simplifying the electrical circuit. The time between pulses is on the order of

Received March 21, 1998; revision received Sept. 21, 1998; accepted for publication Sept. 29, 1998.

*Ph.D., Department of Aeronautical and Astronautical Engineering; currently at 8445 Sutterfield Drive, Colorado Springs, CO 80920. Member AIAA.

†Professor, Department of Aeronautical and Astronautical Engineering. Associate Fellow AIAA.

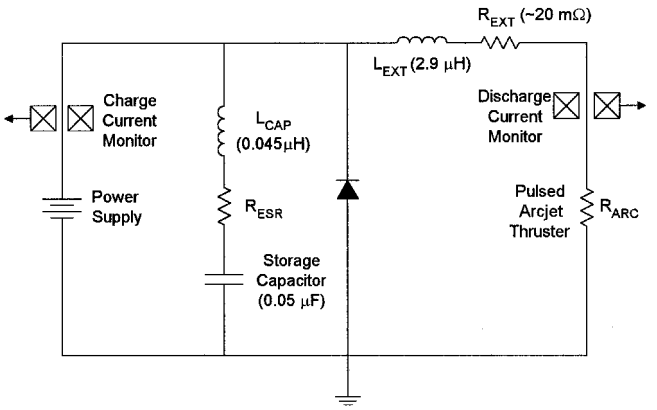

Fig. 1 Electrical diagram of the pulse-forming electrical circuit, including internal resistance R_{ESR} and inductance L_{CAP} of the capacitor.

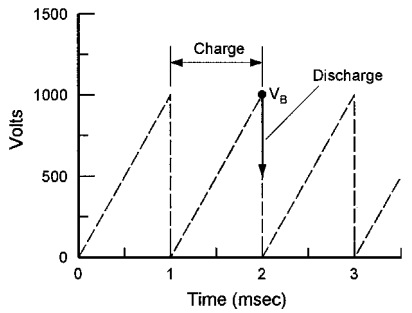

Fig. 2 Schematic of the ideal capacitor voltage for a series of pulses at 1000 pps. The discharge occurs on a time scale that is short compared with the charge time.

1 ms, which is much longer than the arc discharge time of 3–10 μs, so that the arc is present for only a small fraction of the total cycle time. Peak arc currents are 110–270 A, and arc voltages are typically 100–200 V.

Experimental Apparatus

Mechanical Design

The thruster design is based on a NASA 1-kW laboratory-type arcjet,[4] with modifications to the thruster head for pulsed operation, specifically a cylindrical insulator tube called a capillary between the cathode and the anode/nozzle (Fig. 3). The anode is a 20-deg half-angle conical nozzle fabricated from 2%-thoriated tungsten. The nozzle throat was machined using an electron-discharge-machining process to 0.38 mm diameter, measured from a photomicrograph. Two nozzles with area ratios of 20 and 230 were fabricated to evaluate the tradeoff between additional gas expansion vs viscous friction losses because throat Reynolds numbers are typically low, ~1000. Capillary lengths from 5.0 to 12.5 mm were selected so that electrical breakdown would occur at voltages from 1–2 kV for the desired range of mass flow rates.

Propellant gas is injected continuously into the capillary through a 0.28-mm-diam axial orifice in the flat-tipped cathode. The size of the inlet orifice is smaller than the nozzle throat diameter to limit the amount of gas that is blown back upstream after each arc discharge. Using the 1-kW NASA arcjet body for the pulsed arcjet at < 200 W resulted in a nonoptimized thermal design, such that the steady-state temperature of the tungsten nozzle was generally less than 800 K. The measured experimental performance was therefore significantly lower than could be achieved with a more optimized thermal design.

Pulse-Forming Electrical Circuit

During the discharge, the time duration of the arc and the shape of the current pulse are determined by the characteristics of the arc resistance and the configuration of the external electrical circuit. The pulse-forming electrical circuit was designed to provide a nonreversing current pulse, which minimizes energy losses in the capacitor and also benefits capacitor life. The circuit consists of a single-storage capacitor, a high-voltage/high-current diode, and an inductor. The capacitance together with the breakdown voltage determine the pulse energy delivered to the mass of the propellant in the capillary. The all-film dielectric capacitors (0.05 μF) have a maximum voltage rating of 2500 V and a maximum dissipation factor less than 0.0002. The dissipation factor D_F is used to estimate energy losses in the capacitor based on its equivalent series resistance according to the equation $R = D_F/2\pi fC$. The inductance in the circuit (2.90 μH) determines the magnitude of the peak current and the time duration of the arc. The diode, used to eliminate oscillations in the discharge current, has a maximum reverse voltage rating of 3600 V and a 3-V-maximum forward-voltage drop. The diode is heat-sink mounted as close as possible to the capacitor terminals to minimize inductance on the capacitor side of the circuit.

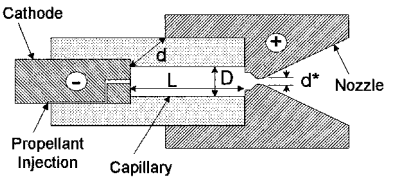

Fig. 3 Schematic of the pulsed arcjet thruster head, including cathode, capillary, and nozzle.

Test Equipment

The thruster is operated in a 1.0-m-diam × 1.5-m-long vacuum tank evacuated to ~50 mtorr with the thruster running. Helium propellant supplied at room temperature from a high-pressure gas cylinder (99.995% purity) flows through a regulator valve to a Unit Instruments model UFC-1500A (5 slm) flow controller, calibrated to an accuracy of better than 2.7% using a control volume method. Power is supplied through a high-voltage coaxial power cable from a constant-current, switching-type power supply (Converter Power Model RCS 3000), which provides a series of charging cycles to the storage capacitor. A separate control circuit reduces variations in the pulse rate caused by coupling between the pulse rate and breakdown voltage.

An inverted pendulum thrust stand is used for thrust measurements.[4] Only the average thrust is observed in the measurement because the pulse rate is three orders of magnitude greater than the thrust-stand natural frequency, and the individual impulse bits are not observed in the thrust measurement. Thrust calibration is performed before and after each test with a pulley arrangement providing three known force levels. A proportional-integral-derivative (PID) controller is used for feedback control.[5] A 12-bit data acquisition card (Keithley Metrabyte DAS-1802HC) installed in a 486 personal computer is used to record four operating parameters: thrust, mass flow rate, breakdown voltage, and pulse rate at a 2-Hz sampling rate. Input power is determined from the measurements of pulse rate and stored energy at breakdown, $P = (\frac{1}{2}CV_B^2)$ (PPS). The signals are processed and displayed in real-time, allowing continuous evaluation of the thruster operating characteristics. The experimental uncertainties are $T \pm 1.9\%$, $P \pm 4.1\%$, $I_{sp} \pm 3.3\%$, and $\eta \pm 6.2\%$, and are discussed in Ref. 6. For detailed measurements related to individual arc pulses and charging cycles, a 4-channel, 8-bit, 10-MHz digital oscilloscope (Soltec) is used. Two inductive current monitors (Pearson models 411 and 4100) are used to measure the capacitor charging current and the arc discharge current. The power supply provides a 0–10 V analog signal proportional to output voltage.

Gasdynamic Theory and Model

The propellant gas flow in the pulsed arcjet is viscous, time-dependent, chemically reacting, two-dimensional axisymmetric, and has time-varying boundary conditions. This complex fluid-flow problem is simplified by treating it as a time-dependent blowdown process from a fixed reservoir (the capillary) through a nozzle. A

time-marching numerical procedure is used in which the pressure and temperature in the capillary are used as upstream boundary conditions to the nozzle. The conditions in the capillary are assumed to be spatially uniform, axially and radially, and both the capillary and nozzle are assumed to be in local thermodynamic equilibrium. The run time for the Fortran computer code is several minutes on a 486 personal computer.

Capillary Boundary Condition

The capillary pressure and temperature are calculated using equations for a uniform-state, uniform-flow thermodynamic process. The mass and energy (m, E) in the capillary are updated at sequential time steps based on the conservation equations [Eqs. (1) and (2)]. The pressure and temperature are then calculated from the specific energy and density. The inlet mass flow is calculated based on a pressure difference across the capillary inlet orifice, and the exit mass flow is determined using equations for choked-flow.[6] The arc discharge is incorporated as a time-dependent energy source Q_{ARC} uniformly distributed to the gas in the capillary. A linear approximation to the arc current pulse, described later, is calculated from the external circuit parameters, pulse energy, and arc voltage, to obtain $Q_{\mathrm{ARC}} = I(t)V_{\mathrm{ARC}}$. Heat transfer from the propellant gas to the capillary wall Q_{LOSS} is determined empirically.[6] For step Δt

$$m^{t+\Delta t} = m^t + (\dot{m}_{\mathrm{IN}} - \dot{m}_{\mathrm{OUT}})\Delta t \tag{1}$$

$$E^{t+\Delta t} = E^t + \left[\dot{m}_{\mathrm{IN}}\left(h_{\mathrm{IN}} + \frac{u_{\mathrm{IN}}^2}{2}\right) - \dot{m}_{\mathrm{OUT}}\left(h_{\mathrm{OUT}} + \frac{u_{\mathrm{OUT}}^2}{2}\right) + Q_{\mathrm{ARC}} - Q_{\mathrm{LOSS}}\right]\Delta t \tag{2}$$

Nozzle Flowfield

The five primary variables in the nozzle calculation are the gas pressure, temperature, density, specific energy, and velocity (p, T, ρ, e, and u, respectively). The three conservation equations give the three flow properties, ρ, u, and e, and the remaining flow properties (p and T) are calculated from the ideal gas law and the Saha equation. The conservation equations of mass, momentum, and energy for unsteady, quasi-one-dimensional flow are written in differential form:

$$\frac{\partial \rho}{\partial t} = \frac{-1}{A}\frac{\partial}{\partial x}(\rho u A) \tag{3}$$

$$\frac{\partial u}{\partial t} = -u\frac{\partial u}{\partial x} - \frac{1}{\rho}\frac{\partial p}{\partial x} - \frac{u^2}{2}\frac{4f}{D} \tag{4}$$

$$\frac{\partial e}{\partial t} = -u\frac{\partial e}{\partial x} - \frac{p}{\rho}\frac{\partial u}{\partial x} - \frac{pu}{\rho A}\frac{\mathrm{d}A}{\mathrm{d}x} + q_{\mathrm{FR}} + q_{\mathrm{NOZ}} \tag{5}$$

The q_{FR} term represents the conversion of kinetic energy into thermal energy caused by friction, and q_{NOZ} is the heat transfer from the gas to the nozzle wall. Ohmic heating in the arc and heat transfer in the capillary are incorporated in the upstream boundary condition, and so these terms do not appear in the nozzle equations. The friction factor is calculated based on a local Reynolds number, and heat transfer is determined empirically,[6] based on a constant Nusselt number.

The gasdynamic model uses the MacCormack predictor–corrector finite difference algorithm, applied successfully by Anderson,[7] to study time-dependent chemically reacting flows in nozzles. The pulsed arcjet grid geometry consists of a 45-deg half-angle conical converging section, a throat region with a constant radius of curvature (2 mm), and a 20-deg half-angle conical diverging section. For most calculations, 50 grid points are used, although sample calculations with up to 200 grid points were performed to verify grid independence. The size of each time step is set by numerical stability limitations and is calculated using a Courant–Friedrichs–Lewy number equal to 0.8. For the boundary condition at the nozzle exit plane, the flow properties are extrapolated from interior points with the restriction that the flow is supersonic. A typical numerical result at 3000 pps is shown in Fig. 4.

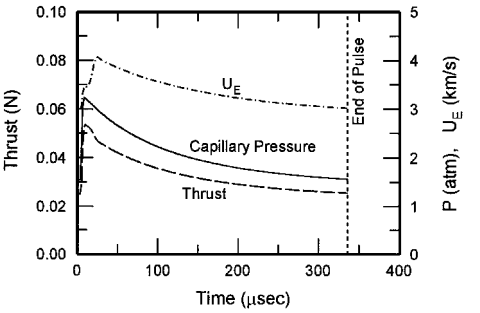

Fig. 4 Typical numerical calculation for thrust, capillary pressure, and exhaust velocity during a single pulse.

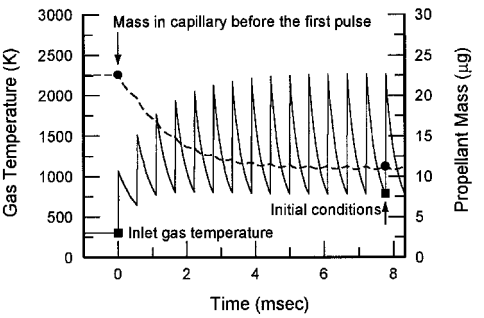

Fig. 5 Numerical results for the propellant mass and gas temperature in the capillary during a typical startup series of pulses at 1800 pps.

Initial Conditions

Before the first pulse, the pressure in the capillary is established by steady choked-flow at a specified mass flow rate. When the first pulse occurs, the gas pressure and temperature in the capillary increase based on the arc energy and the initial propellant mass. The pressure and temperature then decrease monotonically on a time scale that is slightly longer than the time between pulses. At kilo-Hertz pulse rates, the second pulse occurs before conditions in the capillary return to the original starting conditions, such that energy addition from the second discharge starts at a higher initial temperature than the first discharge. The capillary flow conditions converge to a repeatable series after approximately ~10–20 pulses, as shown in Fig. 5. The average propellant mass in the capillary after the series of startup pulses is approximately one-half of the initial propellant mass, leading to higher peak temperatures than would be predicted if the starting series of pulses were not accounted for.

Gasdynamic Model Results

The numerical model was used to evaluate the relative importance of various design and operating parameters. Results from the numerical model indicate that the performance is insensitive to many parameters, including nozzle throat diameter, capillary length and diameter, pulse width, and pulse peak power. The nozzle and capillary wall temperatures are the dominant variables affecting performance. The model predicts that efficiency can be increased to 62% at 401 s I_{sp} by improving the thermal design to reach 1400 K wall temperatures. Interestingly, the average thrust and I_{sp} were insensitive to even large changes in the shape of the current pulse. The rate of energy input to the propellant is controlled by the value of the external circuit inductance, which was varied over two orders of magnitude (2.9–290 μH). This had the effect of decreasing the peak power from 18.4 to 1.7 kW, while lengthening the pulse width from 6.3 to 50 μs. Even though the peak thrust decreases by 14%, the total impulse-bit is identically 11.0 μN-s for both cases. Hence, high peak-power levels are neither an advantage nor a disadvantage under these conditions.

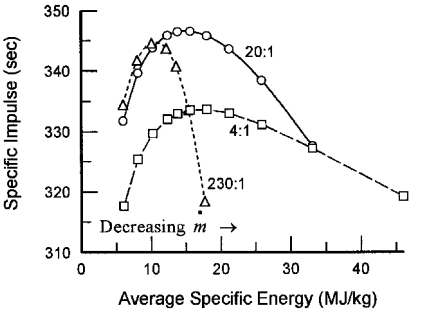

Fig. 6 Specific impulse vs average specific energy for three nozzle area ratios at 120 W, 4000 pps with 1000 K wall temperatures.

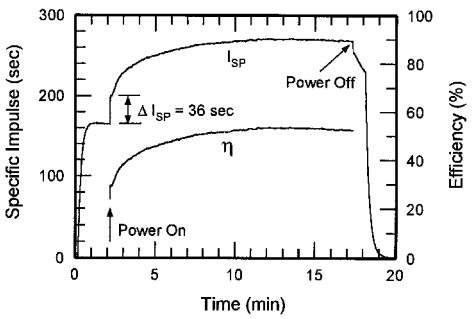

Fig. 7 Specific impulse and efficiency during a typical performance test. The initial thrust increase is followed by a gradual rise related to the thruster thermal design.

Pulsed arcjet performance is calculated with the numerical model for three nozzle area ratios (4, 20, and 230) over a range of specific energies (Fig. 6). The specific energy is varied by setting the input power constant at 120 W and changing the propellant flow rate. At constant power, the average specific energy varies roughly with the inverse of the throat Reynolds number, so that increasing the specific energy can be expected to increase viscous effects in the nozzle. For specific energies less than ~10 MJ/kg, the I_{sp} is highest for the 230:1 nozzle, though the 20:1 nozzle is only 2–3 s lower, with gains of 10–15 s over the 4:1 nozzle. Viscous losses are relatively low with the corresponding higher flow rates, and the performance improves with larger area ratios because of the additional expansion of the gas. These results are consistent with the experimental results, where the specific energies are less than 11 MJ/kg, and the I_{sp} is similar between the 20 and 230 area ratio nozzles. The model predicts a rapid decrease in specific impulse for the 230:1 nozzle as a result of viscous effects at specific energies above 10 MJ/kg, with the exit Mach number decreasing to unity at 18 MJ/kg. The 20:1 nozzle maintains the best I_{sp} between 11 and 33 MJ/kg.

Experimental Performance

For each performance test, the procedure is to allow the mass flow rate to reach steady cold-flow conditions with room-temperature gas, and then apply power. Figure 7 shows data from a typical run. In the first several seconds after power is applied, the thrust increases immediately with a proportional increase in I_{sp} of 10–60 s. The thrust and specific impulse then rise gradually as the nozzle heats up to steady-state temperature. Efficiency is calculated from

$$\eta = \frac{I_{\text{spHOT}}^2}{I_{\text{spCOLD}}^2 + (2P/g^2\dot{m})} \tag{6}$$

where the subscripts to I_{sp} refer to whether or not power is applied. Performance results are shown in Figs. 8 and 9 for 6.6 and 10.1 mg/s helium flow rates at thermal steady state. The experimental data for I_{sp} approximately follow a single curve when plotted vs input power, and differences caused by mass flow rate and nozzle area ratio are within the experimental error. The plotted curves are the performance values predicted by the numerical model, which generally

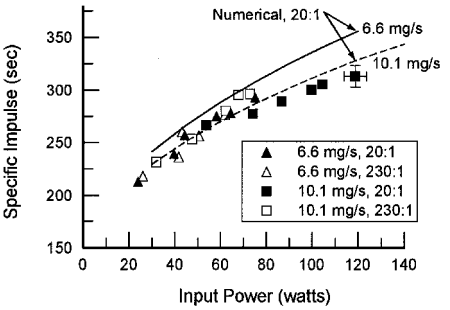

Fig. 8 Specific impulse vs input power for helium at two flow rates (6.6 and 10.1 mg/s) and two nozzle area ratios (20 and 230).

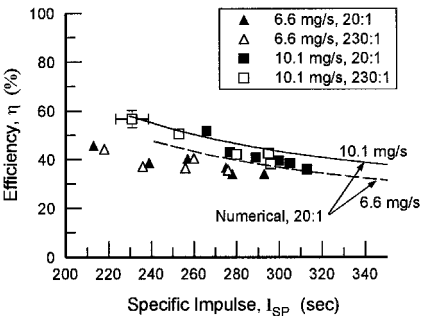

Fig. 9 Experimental and numerical efficiency vs specific impulse.

follow the experimental trends. The numerical results indicate that decreasing the mass flow rate from 10 to 6.6 mg/s at a fixed power level improves the I_{sp} by 15–30 s, consistent with the higher average enthalpy of the gas at the lower mass flow rate.

The experimental data and numerical results show an upward shift in efficiency at a higher flow rate (Fig. 9). This trend is also characteristic of other electrothermal devices, such as dc arcjets, and is generally attributed to decreased frozen-flow loss. However, for the pulsed arcjet running on helium propellant, the frozen ionization losses are small. Further, because the efficiencies appear to be independent of area ratio, the increase in I_{sp} at higher mass flow rates is probably caused by energy-loss effects in the capillary rather than viscous or ionization losses.

Capillary Arc

Breakdown Processes

The arc discharge initiates when the capacitor voltage reaches the prerequisite conditions for Paschen breakdown. Utilizing the self-breakdown voltage to initiate the arc discharge eliminates the need for a separate igniter circuit. However, this technique couples the breakdown voltage to the mass flow rate through the gas number density. This coupling places some restrictions on thruster operation because the input power and the mass flow rate cannot be specified independently, with the ultimate result that the gas enthalpies and peak temperatures tend to be relatively high, even for helium, which breaks down at relatively low voltages. Breakdown is achieved relatively easily in helium, in spite of its high ionization potential, because there are few low-energy states, and electrons can build up to ionization potential over a number of mean free paths without losing energy though elastic collisions.

Paschen breakdown is generally expressed as $V_B = f(nd)$, where d is the minimum electrode separation distance. In conventional breakdown tests, the breakdown distance is identical to the arc length L, but in this particular geometry, the two parameters are different because of the presence of the boron nitride insulator. Voltage breakdown is governed by the electric field strength at the corner of the cathode, and the electric field strength is governed by d, rather than L. Experimental results for breakdown voltage are shown in Fig. 10, where the data were obtained at a low (< 10 pps) pulse rate. Experimentally, it is observed that the breakdown voltage correlates with the minimum electrode separation distance, even though the

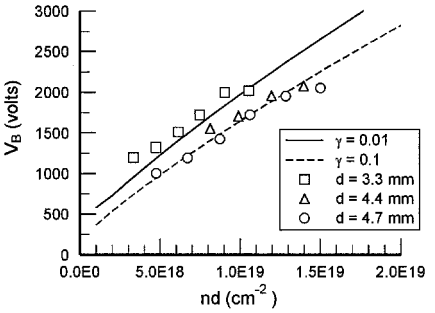

Fig. 10 Experimental breakdown voltage in helium for three values of the electrode separation distance d compared with Eq. (8).

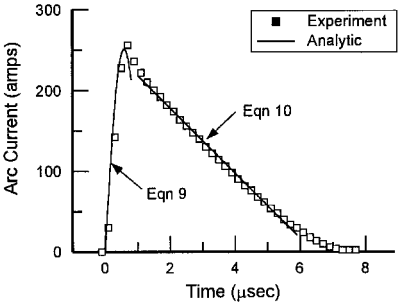

Fig. 11 Experimental data for arc current compared with Eqs. (10) and (11), assuming constant arc voltage.

distance is through the capillary wall. In the Paschen expression [Eq. (7)], V_B is in volts, and the product of nd is given in units of cm^{-2}:

$$V_B = \frac{68.9 \times 10^{-17} nd}{\ell n(15.2 \times 10^{-18} nd)/\ell n(1/\gamma)} \tag{7}$$

The ability to decouple the breakdown distance from the arc distance is a potentially useful technique, particularly for propellants with unfavorable breakdown characteristics. A combination of a long arc length and short breakdown distance allows a lower peak gas temperature than would otherwise be obtained.

Circuit Equations

From a gasdynamic standpoint, the shape of the current pulse has only a minor effect on fluid flow because the arc discharge occurs on a time scale that is much shorter than the characteristic flow time. However, the shape of the current pulse affects the amount of energy lost in the external circuit, and is likely to be an important parameter for the long-term erosion characteristics of the electrodes and for capacitor life. The arc current pulse shape is established by the characteristics of the pulse-forming electrical circuit and the arc resistance. Considering the circuit in Fig. 1 and ignoring the diode for the moment, the circuit behaves similarly to (but not exactly as) a simple LCR circuit. The circuit equation can be written

$$V_B - \frac{1}{C}\int_0^t I\,\mathrm{d}t - (L_{\text{EXT}} + L_{\text{ARC}})\frac{\mathrm{d}I}{\mathrm{d}t} - \left(R_{\text{EXT}} + \frac{\mathrm{d}L_{\text{ARC}}}{\mathrm{d}t}\right) \times I - R_{\text{ARC}} I = 0 \tag{8}$$

Solving this equation requires determining an analytical form for the arc resistance R_{ARC}. A number of models for predicting the resistance in a transient arc discharge can be found in the literature, as summarized by Engel et al.[8] One model consistent with the pulsed arcjet data is to assume that the voltage drop across the arc is constant during the pulse. Replacing the arc resistance, R_{ARC} with $V_{\text{ARC}} I^{-1}$, the circuit equation can be solved analytically for the current as shown by Robiscoe et al.[9] and Maier et al.[10] The arc current increases from zero to peak current in approximately 1 μs, and the voltage on the capacitor decreases from the breakdown voltage to zero. During the initial current rise, or half-cycle, current does not flow through the diode, and the solution to the circuit equation is identical to that for the circuit without the diode

$$I(t) = V_0\sqrt{\frac{C}{L_{\text{EXT}}}}\exp\left(\frac{-R_{\text{EXT}}t}{2L_{\text{EXT}}}\right)\sin\left(\sqrt{\frac{1}{L_{\text{EXT}}C}}t\right) \tag{9}$$

where V_0 is equal to the breakdown voltage minus the arc voltage, $V_B - V_{\text{ARC}}$. Approximately 20–30% of the initial stored energy is transferred to the propellant during the initial current rise, and the remaining energy is temporarily stored in the magnetic field of the circuit inductance.

Now consider the circuit with the diode. After the peak current is reached, the capacitor is essentially removed from the circuit, and the current flows through the diode return loop. The circuit equation for this time period is

$$L_{\text{EXT}}\frac{\mathrm{d}I}{\mathrm{d}t} - V_{\text{ARC}} - V_{\text{DIODE}} - V_{\text{EXT}} = 0 \tag{10}$$

where V_{DIODE} is the forward voltage drop of the diode (2–3 V), and V_{EXT} is the voltage drop associated with the external circuit resistance at high frequency ($\sim$20 mΩ). Assuming approximately constant values for the voltages and inductance, the solution to Eq. (10) is a straight line for the arc current in which the slope is proportional to the arc voltage. The analytical results for the arc current fit the experimental current data very well in both regions (Fig. 11). The negative slope region is highly linear, partially justifying the initial assumption of constant V_{ARC}. Energy losses in the capacitor, diode, and high-frequency circuit resistance are found to be 10–15% of the initial stored energy.

Arc Channel Model

The transient arc resistance can be estimated using Ohm's law and experimental values for arc voltage and current. However, this is insufficient information to calculate an arc temperature because the arc radius is not known. Pulse energies in these experiments are too low to produce an arc column that fills the capillary entirely, such that the arc radius is less than the capillary radius. An approximation, called the channel model, suggested by Steenbeck (see Ref. 11), gives self-consistent results for a constant-voltage arc column and is used here. In the channel approximation, the arc is assumed to have a constant temperature and electrical conductivity across the arc radius r_0, which is less than the capillary radius R. Energy is transferred to the arc by ohmic heating and then is transported radially outward by heat conduction. Magnetic pressure effects are neglected because the arc currents induce magnetic pressures on the order of 0.01 atm, which is small compared with the peak gasdynamic pressure of several atmospheres in the discharge. The energy balance in the channel is given by

$$\frac{1}{r}\frac{\mathrm{d}}{\mathrm{d}r}r\left(\kappa\frac{\mathrm{d}T}{\mathrm{d}r}\right) + \sigma(T)E^2 = 0 \tag{11}$$

where E is the electric field. This equation is called the Elenbaas–Heller equation for steady arcs. Strictly speaking, the transient arc discharge requires a time-dependent term in the energy equation. However, if the arc radius is very small, the energy in the discharge is transported radially outward on a time scale that is rapid compared with the discharge time. Hence, using this equation, as is, is essentially a quasisteady approximation. An improvement to this analysis would include the time-dependent energy terms as well as energy losses caused by radiation.

The set of arc column equations[12] allows the arc column characteristics, including arc voltage and arc radius, to be calculated for a specified arc current. Using experimental data for the arc current,

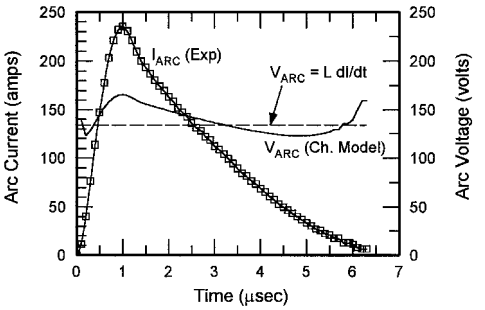

Fig. 12 Arc voltage calculated using data for arc current and the channel model. The channel model agrees closely with the constant arc voltage approximation.

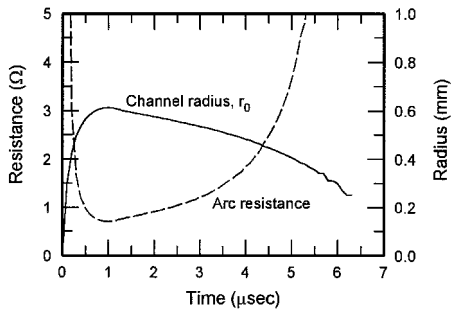

Fig. 13 Arc resistance and channel radius calculated using the channel model. The arc occupies 6–23% of the total capillary volume in the 1.25-mm-radius capillary.

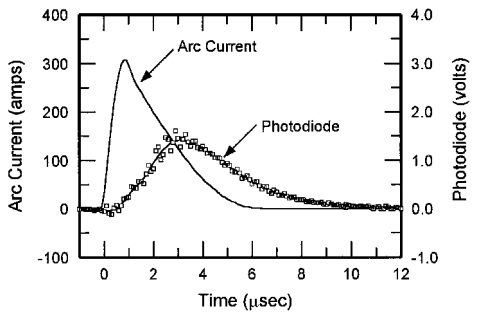

Fig. 14 Photodiode signal and arc current during a pulse. The photodiode response can be interpreted as an indication of the relaxation time in the plasma.

the arc voltage calculated with the channel model (Fig. 12) is relatively constant and agrees well with the value obtained from the slope of the current trace. The time-dependent arc channel radius (Fig. 13) ranges from 0.3 to 0.6 mm in the 1.25-mm-radius capillary, representing 6–23% of the total capillary volume. The peak temperature for this case is 2.0 eV. At higher pulse energies, where the arc fills the capillary, a wall-confined arc model may need to be applied rather than the channel model equations.

Photodiode Measurements

The characteristic relaxation time of the plasma in the capillary was assessed in a simple experiment. A Motorola MRD500 photodiode was placed at the exit plane of the arcjet facing axially into the nozzle throat and the capillary. The photodiode was aligned by hand and was not calibrated, and so the magnitude of the photodiode signal is not used as a diagnostic. The photodiode signal is compared with the arc current measurement in Fig. 14. While the peak current occurs at 0.85 μs, only 24% of the energy has been transferred to the arc during the initial current rise. The peak of the photodiode signal occurs at ~3 μs, after 82% of the pulse energy has been transferred. During the final 3 μs of the arc, the photodiode signal decreases slowly as the power input to the arc is less than the rate of energy loss.

Summary and Conclusions

It has been demonstrated that an electrothermal arcjet, operating in a pulsed mode, can be run on helium propellant with good stability and no low-power limit. Helium is chosen as the propellant to reduce frozen-flow losses and high breakdown voltages found when using hydrazine in this application. Pulsed arcjet fabrication technology is similar to that of a dc arcjet, with the addition of an insulated small-diameter discharge capillary tube located between the anode and cathode. The external circuit typically operates at 1–2 kV, and a small ($\ll$1 J) storage capacitor provides the discharge energy at a rate of several thousand pps. At this frequency, the effect of individual pulses is nearly indistinguishable, and the thrust level at the thruster base is dc. A pulse-forming network prevents current reversal and extends capacitor operating life.

Thrust measurements give a maximum I_{sp} of 313 s at 36% efficiency, at a relatively cool nozzle temperature of 800 K. Results from a numerical model indicate that a thermal redesign to 1400 K nozzle temperatures would increase efficiency with helium propellant to 62% at 401-s I_{sp}. The numerical model also indicates that the primary energy-loss mechanism is heat transfer from the gas to the capillary wall in the subsonic flow region, and these losses depend strongly on wall temperature. Performance is found to be insensitive to many design variables involving capillary and nozzle geometry. Somewhat unexpectedly, performance is found to be insensitive to pulse rate; i.e., 40 MJ pulses at 2000 pps produce the same average thrust as 80 MJ pulses at 1000 pps. At high power (hundreds of watts), performance is not sensitive to the nozzle area ratio, and the performance gains that can be obtained through nozzle optimization are predicted to be small. This result was verified by thrust measurements at area ratios of 20 and 230. At low Reynolds numbers and low power, viscous losses are found to decelerate the flow for large area ratio nozzles, reducing I_{sp}.

The pulse current time–history and circuit energy losses are accurately predicted by assuming that the arc discharge operates at a constant voltage, as was verified by experiment. The arc radius is predicted using the plasma channel model of Elenbaas–Heller, and it is found that the arc diameter is typically 25–50% of the capillary diameter for the pulse energies investigated. The pulse-forming electrical circuit produces energy transfer efficiencies greater than 85% from the capacitor to the arc without current reversals.

The pulsed arcjet can, in principle, be operated with other propellants, and is particularly useful for low-power, high-thrust applications. Specific impulses greater than comparable-size resistojets can generally be expected, because the gas temperature can be raised above the capillary wall temperature, although this wall temperature ultimately limits the maximum performance.

Acknowledgments

This work was supported by a NASA Aerospace Illinois Fellowship. We also acknowledge the Aeronautical and Astronautical Engineering Department of the University of Illinois at Urbana–Champaign for additional funding support.

References

[1]Burton, R. L., Fleischer, D., Goldstein, S. A., and Tidman, D. A., "Experiments on a Repetitively Pulsed Electrothermal Thruster," *Journal of Propulsion and Power*, Vol. 6, No. 2, 1990, pp. 139–144.

[2]Burton, R. L., Hilko, B. K., Witherspoon, F. D., and Jaafari, G., "Energy-Mass Coupling in High-Pressure Liquid-Injected Arcs," *IEEE Transactions on Plasma Science*, Vol. 19, No. 2, 1991, pp. 340–349.

[3]Welle, R. P., "Space Propulsion Applications of Helium Arcjets," AIAA Paper 97-0794, Jan. 1997.

[4]Curran, F. M., and Haag, T. W., "Extended Life and Performance Test of a Low-Power Arcjet," *Journal of Spacecraft and Rockets*, Vol. 29, No. 4, 1992, pp. 444–452.

[5]Black, J. W., Cowie, R. G., Glum, R., and Krier, H., "10kW Laser Propulsion Thruster Test Program Final Report," Phase II SBIR Program, NASA

Contract 3-25636, Dec. 1991.

[6]Willmes, G. F., "A Low Power Pulsed Arcjet Thruster for Spacecraft Propulsion," Ph.D. Dissertation, Univ. of Illinois at Urbana–Champaign, Urbana, IL, May 1997.

[7]Anderson, J. D., "A Time-Dependent Analysis for Vibrational and Chemical Nonequilibrium Nozzle Flows," *AIAA Journal*, Vol. 8, No. 3, 1970, pp. 545–550.

[8]Engel, T. G., Donaldson, A. L., and Kristiansen, M., "The Pulsed Discharge Arc Resistance and Its Functional Behavior," *IEEE Transactions on Plasma Science*, Vol. 17, No. 2, 1989, pp. 323–329.

[9]Robiscoe, R. T., Kadish, A., and Maier, W. B., "A Lumped Circuit Model for Transient Arc Discharges," *Journal of Applied Physics*, Vol. 64, No. 9, 1988, pp. 4355–4363.

[10]Maier, W. B., Kadish, A., and Robiscoe, R. T., "Comparison of the AWA Lumped-Circuit Model of Electrical Discharges with Empirical Data," *IEEE Transactions on Plasma Science*, Vol. 18, No. 6, 1990, pp. 1033–1037.

[11]Peters, T., "Uber den Zusammenhang des Steenbeckschen Minimumprinzips mit dem thermodynamishen Prinzip der minimalen Entropieerzeugung," *Zeitschrift fur Physik*, Vol. 144, 1956, pp. 612–631.

[12]Raizer, Y. P., "Arc Discharges," *Gas Discharge Physics*, Springer–Verlag, Berlin, 1991.